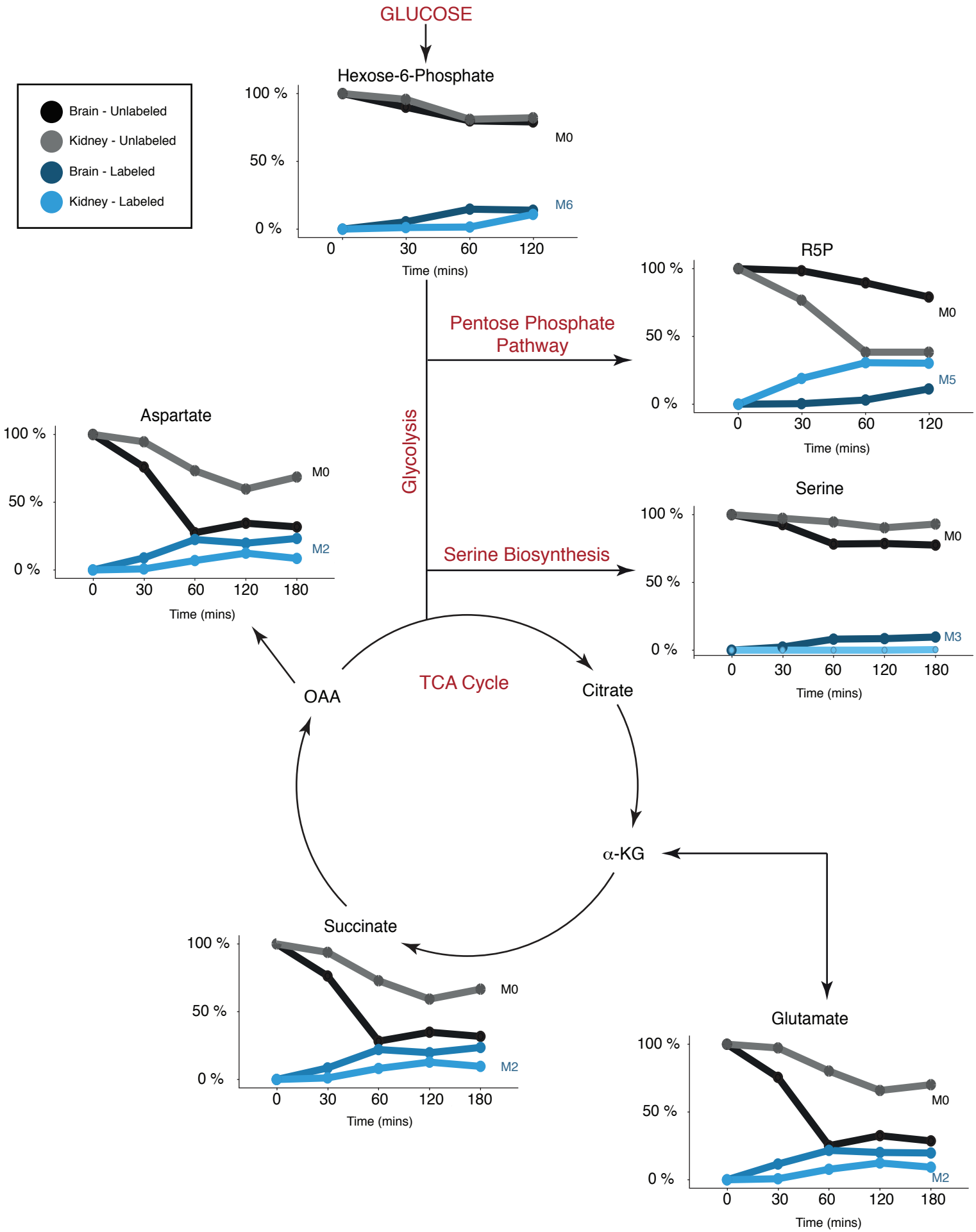

Figure S1 Davidson et al.

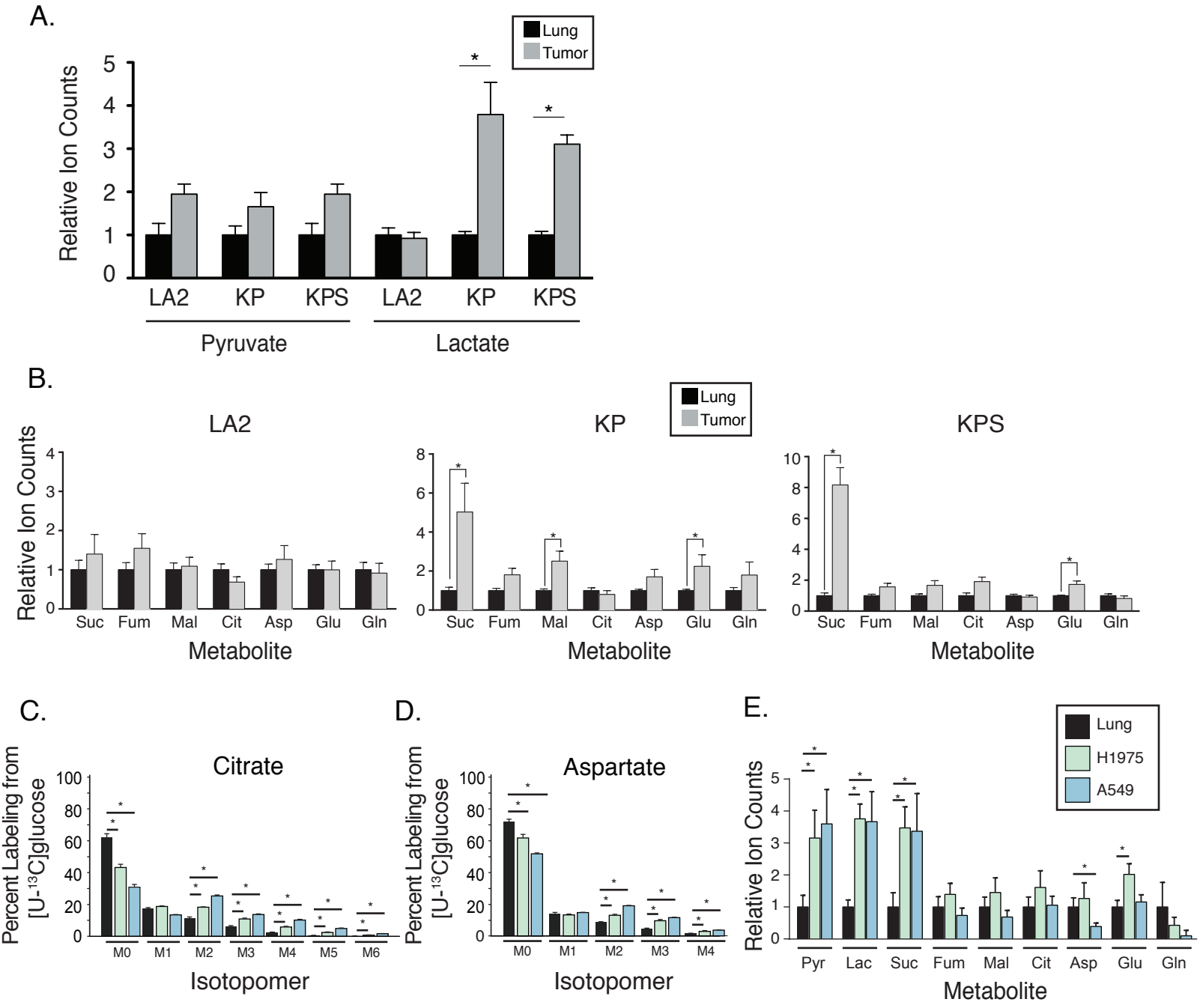

Figure S2 Davidson et al.

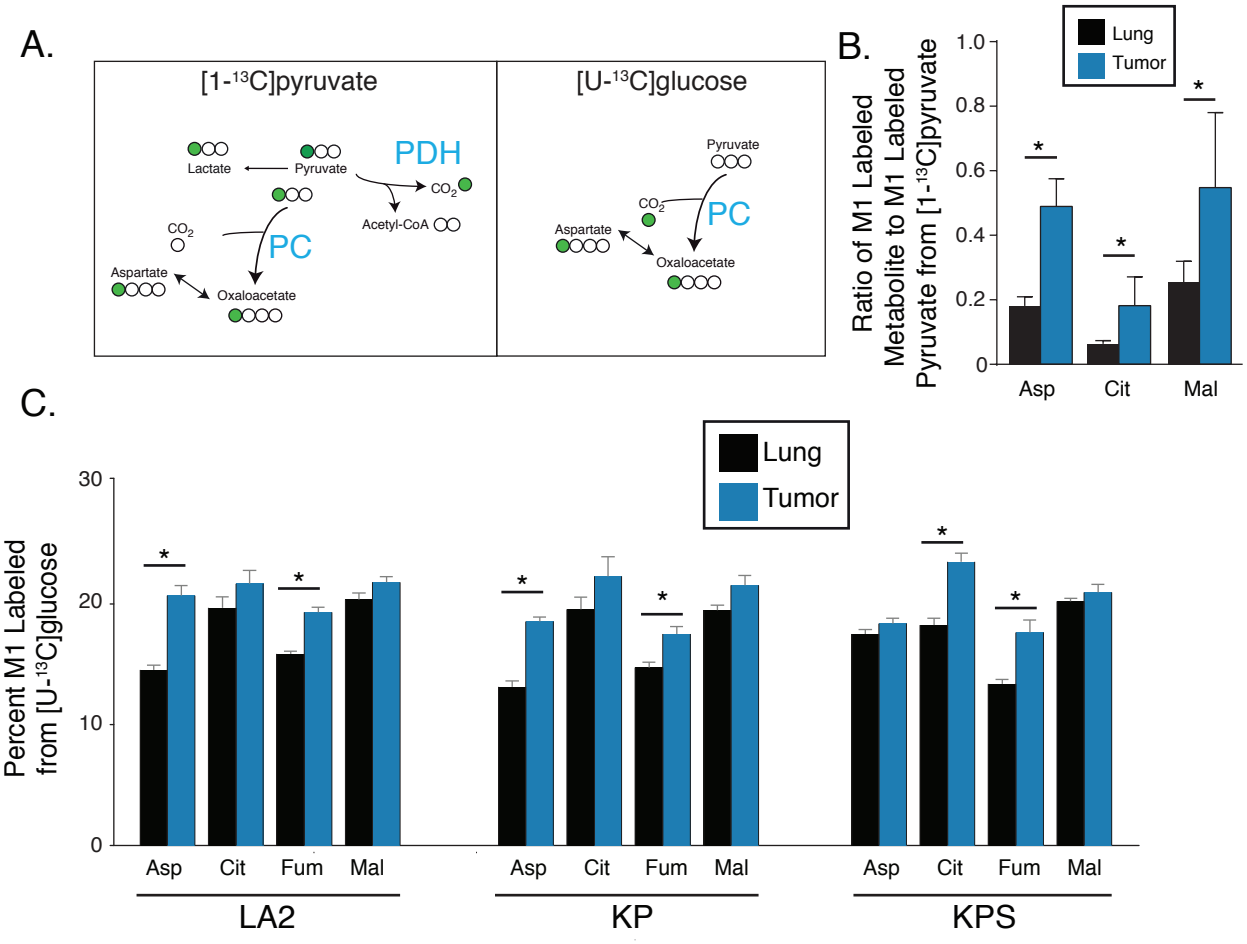

Figure S3 Davidson et al.

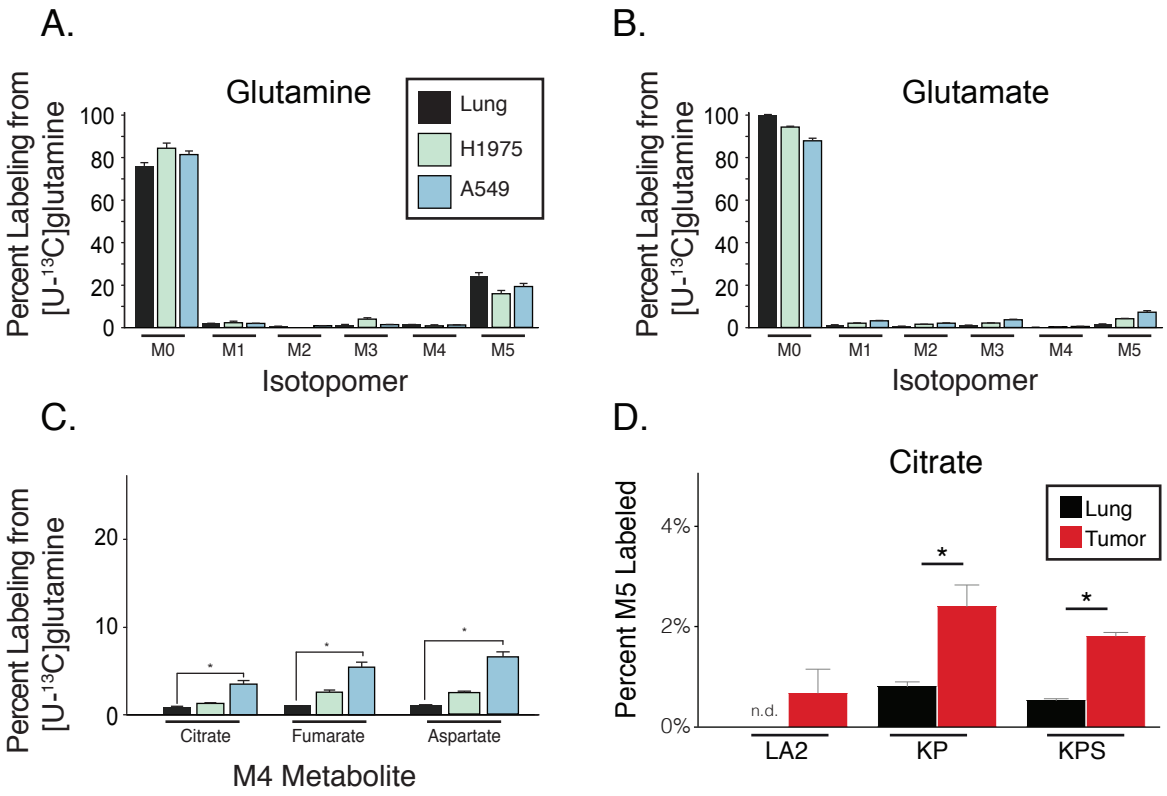

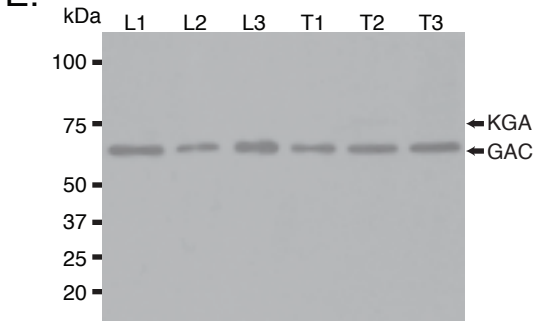

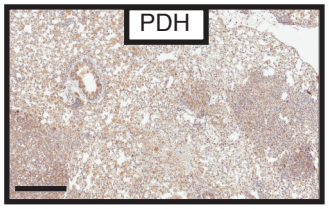

Figure S4 Davidson et al.

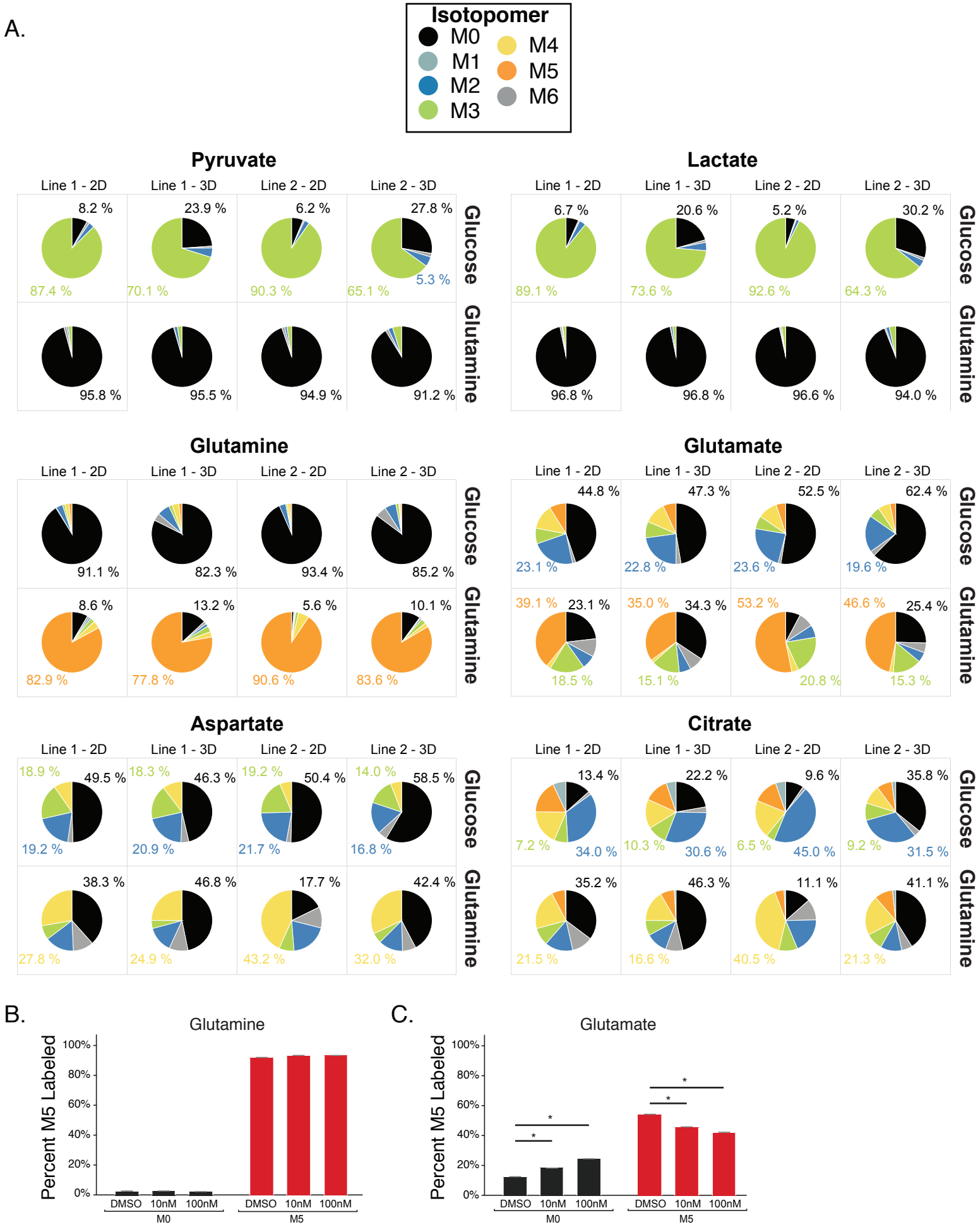

Figure S5 Davidson et al.

A.

Gls1

```
Exon1 5′ GACCTGTCCGGCGGGCGCGGCCCCGGGAAGCGCGCCGGCGGGGGCGGGGTGGTGCCC
Exon1 3′ CTGGACAGGCCGCCCGCGCCGGGGCCCTTCGCGCGGCCGCCCCCGCCCCACCACGGG
                          sgGls1.1          PAM

                                  sgGls1.2          PAM
Exon1 5′ CAGCATTATTTACTCCTTGCTGAAAAGAAATGAAAGGCAAGCATTTTAATACAGACA
Exon1 3′ GTCGTAATAAATGAGGAACGACTTTTCTTTACTTTCCGTTCGTAAAATTATGTCTGT
```

B.

Pdha1

```
Exon1 5′ ATGAGGAAGATGCTTGCCGCTGTATCCCGCGTGTTGGCAGGCTCTGCGCAGAAGCCG
Exon1 3′ TACTCCTTCTACGAACGGCGACATAGGGCGCACAACCGTCCGAGACGCGTCTTCGGC
                                  PAM          sgPdha1
sgPDHE1α 5′ ATGAGGAAGATGCTTGCCGCTGTATCCCGCAT-CTGGCAGGCTCTGCGCAGAAGCCG
```

C.

Pcx

```
                  sgPcx.2          PAM                sgPcx.1          PAM
Exon1 5′ TTGCCTCCCCAAATGTCCGGCGTCTGGAGTATAAGCCTATCAAGAAAGTAATGGTGG
Exon1 3′ AACGGAGGGGTTTACAGGCCGCAGACCTCATATTCGGATAGTTCTTTCATTACCACC

sgPCX.1 5′ TTGCCTCCCCAAATGTCCGGCGTCTGGAGTATAAGCCTATCAAGAAAGT---GGTGG
sgPCX.2 5′ TTGCCTCCCCAAATGTCCCCATTCTCCAGTATAAGCCTATCAAGAAAGTAATGGTGG
                                  TATA
```

K.

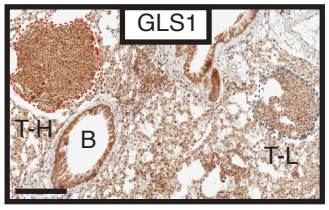

D.

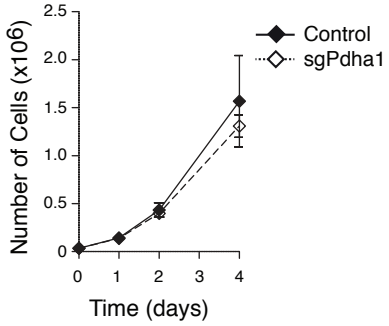

E.

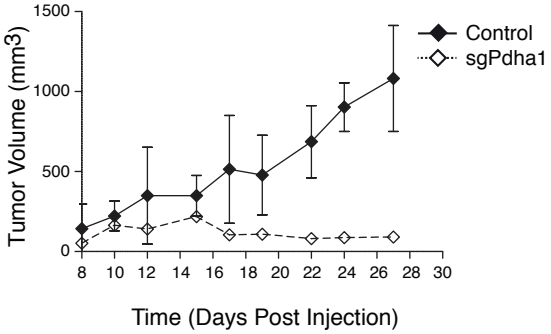

F.

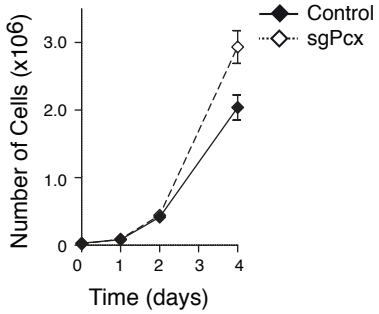

G.

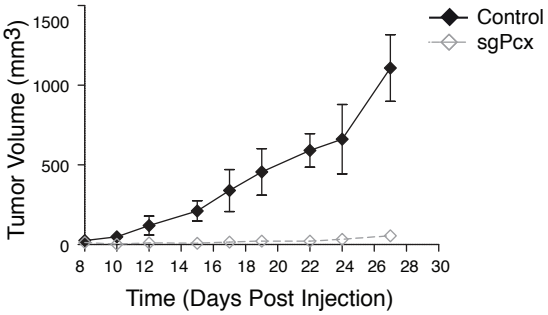

H.

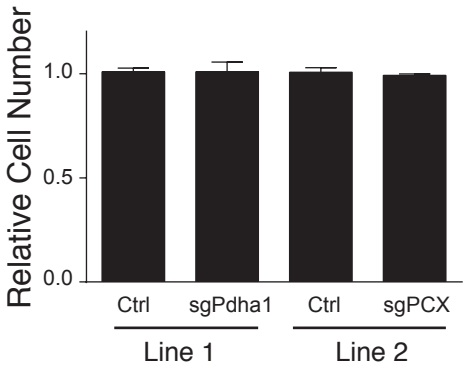

I.

Orthotopic

Tumor Burden	Control	sgPdha1
High	5	0
Medium	0	0
Low	1	1
None	0	4

Orthotopic

Tumor Burden	Control	sgPcx
High	5	0
Medium	0	0
Low	1	1
None	0	5

J.

Autochthonous

Tumor Burden	Control	sgPdha1
High	3	3*
Medium	0	1*
Low	1	0
None	0	0

Autochthonous

Tumor Burden	Control	sgPcx
High	3	0
Medium	1	0
Low	0	1
None	0	4

Figure S6 Davidson et al.

Figure S7 Davidson et al.

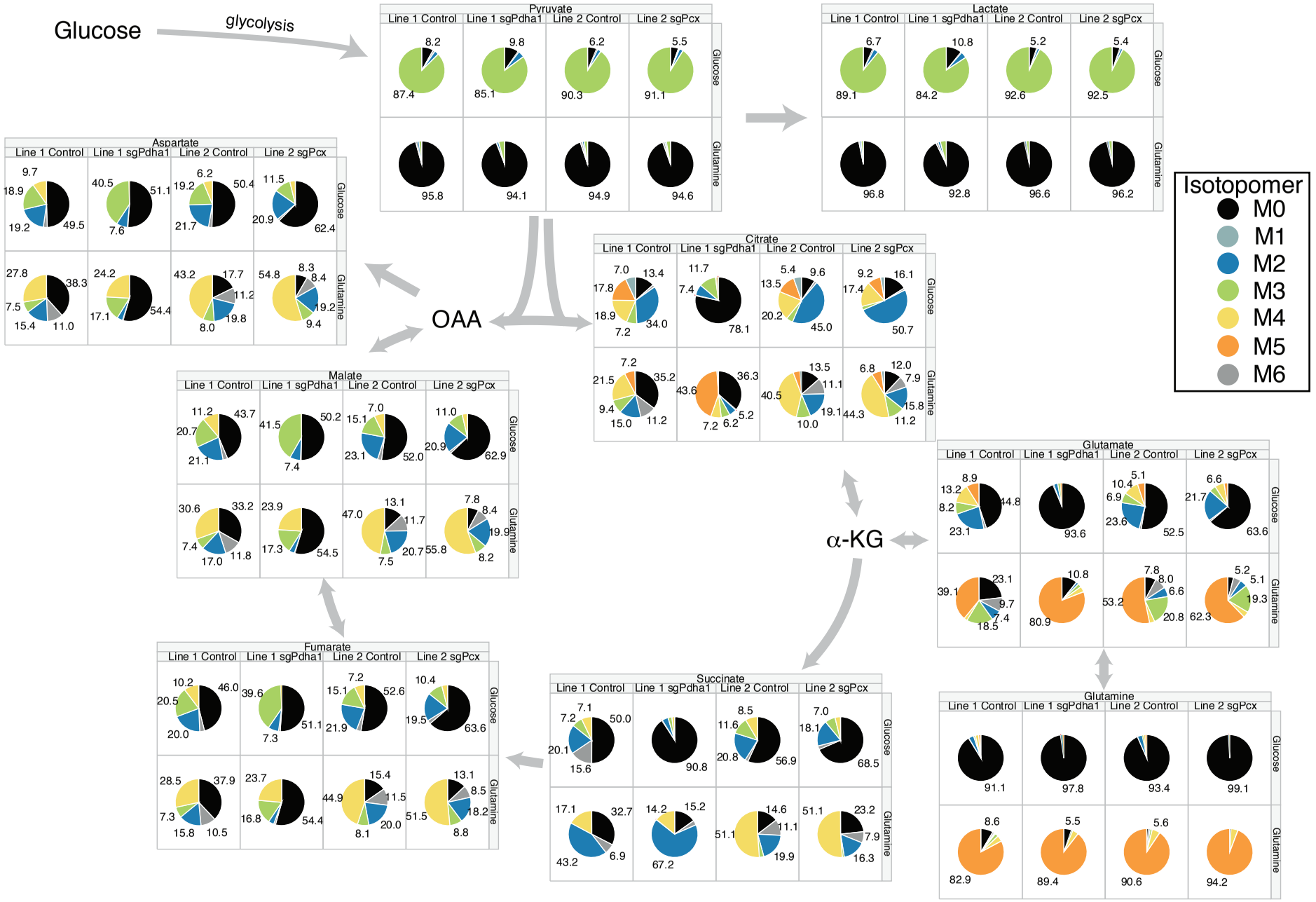

SUPPLEMENTAL INFORMATION

SUPPLEMENTAL FIGURE LEGENDS

Figure S1, Infusion of stable isotope labeled glucose results in isotopic steady state across pathways in the indicated tissue samples, related to Figure 1.

Tissue metabolites of time from animals infused with [U-^{13}C]glucose. The unlabeled species and the dominant expected isotopomer of the indicated metabolite from brain and kidney are displayed.

Figure S2, Relative metabolite concentrations and extended isotopomer distributions of xenograft tumors, related to Figure 2.

(A) Relative abundance of intracellular pyruvate and lactate in lung (black) and adjacent tumor (grey) for the indicated lung tumor models (LA2, n = 8; KP, n = 12; KPS, n = 12). Significantly different values as determined by two-tailed T-test are marked with a *, $p < 0.05$. All values shown represent mean $\pm$ SEM.

(B) Relative abundance of measured intracellular metabolites in lung (black) and adjacent tumor (grey) for the indicated lung tumor models (LA2, n = 8; KP, n = 12; KPS, n = 12). Significantly different values as determined by two-tailed T-test are marked with a *, $p < 0.05$. All values shown represent mean $\pm$ SD.

(C, D) Mass-isotopomer distribution of metabolites of citrate (Cit) and aspartate (Asp) following 6-hour [U-^{13}C]glucose infusion in lung (black) and xenografted tumors H1975 (green) and A549 (blue). (Lung, n = 8; H1975, n = 8; A549, n = 8). Significantly different values as determined by two-tailed unpaired T-test are marked with a *, $p < 0.05$. All values are mean $\pm$ SEM.

(E) Relative abundance of measured intracellular metabolites in lung (black) and xenografted tumors H1975 (green) and A549 (blue). (Lung, n = 8; H1975, n = 8; A549, n = 8). Significantly different values as determined by two-tailed T-test are marked with a *, $p < 0.05$. All values shown represent mean $\pm$ SD.

Figure S3, Assessment of pyruvate carboxylase flux into the TCA cycle using [U-^{13}C]glucose and [1-^{13}C]pyruvate tracers, related to Figure 2.

(A) Schematic showing isotope transitions expected from [1-^{13}C]pyruvate to oxaloacetate and from unlabeled pyruvate incorporating a labeled CO_2 derived from [U-^{13}C]glucose through PC.

(B) Ratio of intratumoral M1 isotopomers of aspartate (Asp), citrate (Cit), and malate (Mal) to M1 labeled pyruvate in lung (black) and KP tumor (blue) following infusion of [1-^{13}C]pyruvate. (Lung, n =

3; KP tumor n=4). Significantly different values as determined by two-tailed unpaired T-test are marked with a *, $p < 0.05$. All values are mean ± SD.

(C) M1 mass-isotopomers of metabolites of aspartate (Asp), citrate (Cit), fumarate (Fum) and malate (Mal) in lung tissue (black) and tumor tissue (blue) following 6-hour [U-^{13}C]glucose infusion. (LA2, n = 4; KP, n = 6; KPS, n = 5). Significantly different values as determined by two-tailed unpaired T-test are marked with a *, $p < 0.05$. All values are mean ± SEM.

Figure S4, Limited glutamine catabolism by xenografted tumors and evidence for reductive carboxylation in tumors from [U-^{13}C]glutamine infusion, related to Figure 3.

(A,B) Mass-isotopomer distribution of glutamine and glutamate in lung tissue (black) and xenograft tissue (H1975, green; A549, blue) following 6-hour [U-^{13}C]glutamine infusion. (Lung n=7, A549 n=6, H1975 n=8). Mean glutamine enrichment was 34.3 (+/- 3.7%). Significantly different values as determined by two-tailed paired T-test are marked with a *, $p < 0.05$. All values are mean ± SEM.

(C) Labeled M4 mass-isotopomer of citrate, fumarate, and aspartate in lung (black) and tumor tissue (H1975, green; A549, blue) following 6-hour [U-^{13}C]glutamine infusion. Significantly different values as determined by two-tailed paired T-test are marked with a *, $p < 0.05$. All values are mean ± SEM.

(D) Labeled M5 mass-isotopomer of citrate in lung tissue (black) and the indicated tumor tissue (red) following 6-hour [U-^{13}C]glutamine infusion. n.d. indicates that the isotopomer was not detected. (LA2, n = 4; KP, n = 4; KPS, n = 4). Significantly different values as determined by two-tailed paired T-test are marked with a *, $p < 0.05$. All values are mean ± SEM.

(E) Western blot analysis of glutaminase (Gls1) expression in three representative KP lung tumors (Tumor) and normal lung tissue from three mice (Lung). Full blot presented to determine if either splice isoform of Gls1, KGA (predicted MW: 75kDa) and GAC (predicted MW: 65kDa), is expressed.

(F) Representative IHC analysis of Pdha1 expression in KP lung tumors and adjacent normal lung tissue.

Figure S5, Glucose and glutamine metabolism by lung cancer cells in 3D culture, related to Figure 4.

(A) Labeling of central carbon metabolites from [U-^{13}C]glucose or [U-^{13}C]glutamine (rows) from KP lung cancer cells cultured in standard cell culture conditions (2D) or in matrigel (3D). The numerical percent labeling is color coded by isotopomer for major isotopomer species, (n=3).

(B,C) The unlabeled M0 and fully labeled M5 isotopomers of glutamine (B) and glutamate (C) from KP-derived lung cancer cells treated with DMSO, 10 nM CB-839 (10 nM), or 100 nm CB-839 (100 nM) are shown.

Figure S6, Targeted gene disruption with CRISPR/Cas9 and effect on cell proliferation and tumor growth, related to Figure 6 and 7.

(A-C), sgRNA design and representative sequencing results showing mutations introduced into isogenic cell lines where *Pdha1*, *Pcx*, *Gls1* are disrupted (guide sequence, blue; protospacer adjacent motif (PAM), green; mutations, red).

(D-E) Cell numbers over time of a Control and sgPdha1 targeted KP cell line in culture (F) and tumor volume measurements over time of the same cell lines allografted into the flanks of C57Bl6 mice (G). Data shown are the mean +/- SEM (n = 4/cell line).

(F-G) Cell numbers over time of a Control and sgPcx targeted KP cell line in culture (D) and tumor volume measurements over time of the same cell lines allografted into the flanks of C57Bl6 mice (E). Data shown are the mean +/- SEM (n = 4/cell line).

(H) Relative tumor burden from orthotopic transplants from control, sgPdha1, and sgPcx or cell lines in the lungs of nu/nu and C57Bl6 mice. Data are based on relative tumor area.

(I) KP lung cancer cells with or without disruption of Pdha1 or Pcx were cultured in matrigel and relative cell numbers assessed after 48 hours (n=3).

(J) Relative tumor burden from autochthonous pSECC experiments from control, sgPdha1 and sgPcx. Data are based on relative tumor area. * denotes that Pdha1 knockout was not observed and that the tumors responsible for the high burden observed in these models retained Pdha1 expression.

(K) Representative IHC analysis of Gls1 expression after delivery of pSECC containing sgGls1 in KP lung tumors and adjacent normal lung tissue. Scale bar = 300μm. (T-H = Tumor High Gls1 Expression, T-L = Tumor Low Gls1 Expression, B = Bronchiole).

Figure S7, [U-^{13}C]glucose and glutamine labeling of metabolites in *Pdha1* and *Pcx* knockout cell lines, related to Figure 6 and 7.

[U-^{13}C]glucose- and glutamine- isotopomers labeling of central carbon metabolites (columns, genetic alterations of either Control, sgPcx, or sgPdha1 cell lines; rows, stable isotope tracer of labeled glucose or glutamine and resulting isotopomers, n=3).

SUPPLEMENTAL TABLES

Table S1 – Detection of Metabolites by GCMS, Metabolite fragments detected with gas chromatography mass-spectrometry (GC-MS), related to Figures 2-5.

Metabolite	Carbons	Formula	Mass (m/z)
Pyruvate	123	C6H12O3NSi	174
Lactate	23	C10H25O2Si2	233
Lactate	123	C11H25O3Si2	261
Citrate	123456	C20H39O6Si3	459

Citrate	123456	C26H55O7Si4	591
αKG	12345	C14H28O5NSi2	346
Succinate	1234	C12H25O4Si2	289
Fumarate	1234	C12H23O4Si2	287
Malate	1234	C18H39O5Si3	419
Alanine	23	C10H26ONSi2	232
Alanine	123	C11H26O2NSi2	260
Aspartate	12	C14H32O2NSi2	302
Aspartate	234	C17H40O3NSi3	390
Aspartate	1234	C18H40O4NSi3	418
Glutamate	12345	C17H36O2NSi2	330
Glutamate	12345	C19H42O4NSi3	432
Glutamine	12345	C19H43O3N2Si3	431

Table S2 ***(Supplemental .xls)*****,** Mass isotopomer distributions for all metabolites from LA2, KP, KPS lung and control tissue, related to Figures 2, 3.

Table S3 - Model used for ^{13}C metabolic flux analysis, Metabolic Flux Analysis Network. Model includes central carbon metabolism and major anabolic pathways. Atom transitions are given in parentheses next to chemical species, related to Figure 4

Extracellular Fluxes and Biomass Production
Glc.x (abcdef) → G6P (abcdef)
Lac (abc) → Lac.x (abc)
Gln.x (abcde) → Gln (abcde)
Glu (abcde) → Glu (abcde)
97.05*Asp.c + 104.85*Glu + 90*Ala + 48.3*Gln + 368.5*AcCoA.c + 17.25*DHAP + 34.395*P5P → Biomass
Glycolysis
G6P (abcdef) ←→ F6P (abcdef)
F6P (abcdef) → DHAP (cba) + GAP (def)
DHAP (abc) ←→ GAP (abc)
GAP (abc) ←→ 3PG (abc)
3PG (abc) → Pyr.c (abc)
Pyr.c (abc) → Lac (abc)
Anaplerotic Fluxes
Pyr.m (abc) + CO2 (d) → Oac.m (abcd)
Mal.m (abcd) ←→ Pyr.m (abc) + CO2 (d)
Glu (abcde) ←→ Akg.m (abcde)
Oac.m (abcd) ←→ Asp.m (abcd)
TCA Cycle
Pyr.m (abc) → AcCoA.m (bc) + CO2 (a)
AcCoA.m (ab) + Oac.m (cdef) → Cit.m (fedbac)
Cit.m (abcdef) ←→ Akg.m (abcde) + CO2 (f)
Akg.m (abcde) → Suc (bcde) + CO2 (f)
Suc (abcd) ←→ Fum (abcd)
Fum (abcd) ←→ Mal.m (abcd)
Mal.m (abcd) ←→ Oac.m (abcd)
Cit.c (abcdef) ←→ Akg.c (abcde) + CO2 (f)
Oac.c (abcd) ←→ Asp.c (abcd)

Fatty and Amino Acids

Cit.c (abcdef) → AcCoA.c (ed) + Oac.c (fcba)
Pyr.m (abc) ←→ Ala (abc)
Gln (abcde) → Glu (abcde)

Mixing and Transport

0*Pyr.c (abc) → Pyr.mnt (abc)
0*Pyr.m (abc) → Pyr.mnt (abc)
0*Mal.c (abcd) → Mal.mnt (abcd)
0*Mal.m (abcd) → Mal.mnt (abcd)
0*Cit.c (abcdef) → Cit.mnt (abcdef)
0*Cit.m (abcdef) → Cit.mnt (abcdef)
0*Asp.c (abcd) → Asp.mnt (abcd)
0*Asp.m (abcd) → Asp.mnt (abcd)
0*Akg.c (abcde) → Akg.mnt (abcde)
0*Akg.m (abcde) → Akg.mnt (abcde)
Pyr.c (abc) ←→ Pyr.m (abc)
Mal.c (abcd) ←→ Mal.m (abcd)
Cit.c (abcdef) ←→ Cit.m (abcdef)
Akg.c (abcde) ←→ Akg.m (abcde)
Asp.c (abcd) ←→ Asp.m (abcd)

Table S4. Estimated fluxes for KP-derived mouse tumor cell line, Estimated fluxes from a [U-^{13}C]glutamine tracer in a KP-derived cell line, related to Figure 4.

Pathway/Reaction	Flux	95% confidence interval	
	(fmol/cell/h)	Lower bound	Upper bound
Extracellular Fluxes and Biomass Production			
Glc.x → G6P	767.2	746.1	790
Lac → Lac.x	1328	1285	1369
Gln.x → Gln	144.6	134.7	153.5
Glu → Glu	82.82	68.78	96.18
97.05*Asp.c + 104.85*Glu + 90*Ala + 48.3*Gln + 368.5*AcCoA.c + 17.25*DHAP + 34.395*P5P → Biomass	0.04648	0.04229	0.05298
Glycolysis			
G6P → F6P	649.7	609.4	689.1
G6P ←→ F6P	1.00E+07	0	Inf
F6P → DHAP + GAP	726.9	704.9	746.6
DHAP → GAP	726.1	704.2	745.6
DHAP ←→ GAP	1.00E-07	0	Inf
GAP → 3PG	1492	1449	1533
GAP ←→ 3PG	-1.76E-05	0	Inf
3PG → Pyr.c	1492	1449	1533
Pyr.c → Lac	1328	1285	1369
Pyr.c ←→ Lac	1.07E+05	0	Inf
Pentose Phosphate Pathway			
G6P → P5P + CO2	117.4	72.93	159.4
P5P + P5P → S7P + GAP	38.61	23.78	52.59
P5P + P5P ←→ S7P + GAP	1.00E+07	2.146	Inf
S7P + GAP → F6P + E4P	38.61	23.78	52.59
S7P + GAP ←→ F6P + E4P	5.98E+01	2.292	106.9
P5P + E4P → F6P + GAP	38.61	23.78	52.59
P5P + E4P ←→ F6P + GAP	1.10E-07	0	97.31

Anaplerotic Fluxes			
Pyr.m + CO2 → Oac.m	19.73	16.52	21.52
Mal.m → Pyr.m + CO2	69.85	64.35	80.2
Mal.m ←→ Pyr.m + CO2	9.17E-08	0	3.269
Glu → Akg.m	54.62	45.16	64.01
Glu ←→ Akg.m	5835	3577	1.26E+04
Oac.m → Asp.m	-12.62	-14.38	-11.48
Oac.m ←→ Asp.m	1.00E+07	1265	Inf
TCA Cycle			
Pyr.m → AcCoA.m + CO2	210.1	195.7	223.2
AcCoA.m + Oac.m → Cit.m	210.1	195.7	223.2
Cit.m → Akg.m + CO2	206.2	-22.68	250
Cit.m ←→ Akg.m + CO2	1.274	0	25.15
Akg.m → Suc + CO2	247.6	230.9	263.1
Suc → Fum	247.6	230.9	263.1
Suc ←→ Fum	1.60E-03	0	Inf
Fum → Mal.m	247.6	230.9	263.1
Fum ←→ Mal.m	1.00E+07	831.2	Inf
Mal.m → Oac.m	177.7	164.3	184.8
Mal.m ←→ Oac.m	346	265.7	569.6
Cit.c → Akg.c + CO2	-13.25	-46.95	219.9
Cit.c ←→ Akg.c + CO2	1.00E+07	17.41	Inf
Oac.c → Asp.c	17.13	15.58	19.52
Oac.c ←→ Asp.c	3.99E-04	0	Inf
Fatty and Amino Acids			
Cit.c → AcCoA.c + Oac.c	17.13	15.58	19.52
Pyr.m → Ala	4.183	3.806	4.769
Pyr.m ←→ Ala	-1.75E-06	0	Inf
Gln → Glu	142.3	132.5	151.1
Mixing and Transport			
0*Pyr.c → Pyr.mnt	1.00E-07	0	0.7424
0*Pyr.m → Pyr.mnt	1	0.2576	1
0*Mal.c → Mal.mnt	1	0	1
0*Mal.m → Mal.mnt	1.00E-07	0	1
0*Cit.c → Cit.mnt	0.1371	0	0.169
0*Cit.m → Cit.mnt	0.8629	0.831	1
0*Akg.c → Akg.mnt	1.00E-07	0	1
0*Akg.m → Akg.mnt	1	0	1
0*Asp.c → Asp.mnt	0.4786	0	1
0*Asp.m → Asp.mnt	0.5214	0	1
Pyr.c → Pyr.m	164.1	146.7	180.8
Pyr.c ←→ Pyr.m	5924	2619	4.60E+04
Mal.c → Mal.m	-1.42E-17	0	0
Mal.c ←→ Mal.m	1.00E-07	0	Inf
Cit.c → Cit.m	-3.878	-237.7	29.81
Cit.c ←→ Cit.m	1.00E-07	0	43.38
Akg.c → Akg.m	-13.25	-46.95	219.9
Akg.c ←→ Akg.m	1.00E-07	0	4588
Asp.c → Asp.m	12.62	11.48	14.38
Asp.c ←→ Asp.m	1.00E+07	9.107	Inf

Sum of squared errors (SSE) = 38.5

Expected SSE = [34.0, 73.8] (95% confidence interval, 52 degrees of freedom)

Table S5. Measured and simulated extracellular fluxes (all units in fmol cell^{-1} h^{-1}, except specific growth rate in h^{-1}), Extracellular fluxes for a KP-derived cell line, related to Figure 4.

Flux	Measured	Simulated
Glucose consumption	757.42 ± 28.05	767.156
Lactate production	1331.26 ± 23.53	1327.564
Glutamine consumption	145.56 ± 5.15	144.5669
Specific growth rate	0.0451 ± 0.0037	0.04648

Table S6. Measured and simulated [U-^{13}C]glutamine metabolite labeling patterns, Mass isotopomers used to determine flux in central carbon metabolism from [U-^{13}C]glutamine tracer in a KP-derived cell line, related to Figure 4.

Fragment	Mass Isotopomer	Measured	Simulated
Pyr174	M+0	0.81793	0.818803
	M+1	0.11397	0.111541
	M+2	0.04597	0.04485
	M+3	0.02077	0.021777
	M+4	0.00103	0.002197
	M+5	0.00037	0.000791
Lac233	M+0	0.735	0.733309
	M+1	0.1651	0.168281
	M+2	0.08333	0.082101
	M+3	0.01263	0.012988
	M+4	0.00327	0.002955
	M+5	0.0005	0.000323
Lac261	M+0	0.72087	0.722322
	M+1	0.17357	0.171471
	M+2	0.0737	0.075155
	M+3	0.02537	0.024616
	M+4	0.00493	0.004848
	M+5	0.00143	0.001381
	M+6	0.0002	0.000173
Ala260	M+0	0.71827	0.715309
	M+1	0.16823	0.174218
	M+2	0.07667	0.075126
	M+3	0.02913	0.027957
	M+4	0.00583	0.005508
	M+5	0.00173	0.001639
Mal419	M+0	0.1346	0.138238
	M+1	0.1501	0.153792
	M+2	0.1917	0.198108
	M+3	0.1064	0.098267
	M+4	0.28167	0.275624
	M+5	0.08627	0.085666
Asp302	M+0	0.30557	0.304277
	M+1	0.1653	0.168677
	M+2	0.39157	0.389753

	M+3	0.09323	0.095654
	M+4	0.037	0.035044
	M+5	0.0066	0.005559
Asp390	M+0	0.17967	0.179949
	M+1	0.20433	0.205478
	M+2	0.16573	0.162493
	M+3	0.30093	0.30187
	M+4	0.0948	0.097386
	M+5	0.04093	0.041566
Asp418	M+0	0.15773	0.154061
	M+1	0.1555	0.156209
	M+2	0.19053	0.192526
	M+3	0.1083	0.105881
	M+4	0.25717	0.261587
	M+5	0.08457	0.082597
Glu330	M+0	0.12697	0.12581
	M+1	0.15707	0.154971
	M+2	0.20567	0.207527
	M+3	0.0737	0.075048
	M+4	0.324	0.32319
	M+5	0.07683	0.077808
Glu432	M+0	0.0984	0.098168
	M+1	0.11797	0.116015
	M+2	0.09813	0.095581
	M+3	0.16957	0.171304
	M+4	0.07297	0.075308
	M+5	0.29583	0.296246
Cit459	M+0	0.13567	0.140506
	M+1	0.15373	0.149805
	M+2	0.17957	0.179224
	M+3	0.12093	0.122931
	M+4	0.22937	0.230254
	M+5	0.10993	0.110018
	M+6	0.0506	0.048539
Cit591	M+0	0.12087	0.120794
	M+1	0.1453	0.143205
	M+2	0.17823	0.174405
	M+3	0.12923	0.129679
	M+4	0.21503	0.217246
	M+5	0.12273	0.122973
	M+6	0.06073	0.061443

Table S7. Measured and simulated [1,2-^{13}C]glucose metabolite labeling patterns, Mass isotopomers used to determine flux in PPP from [1,2-^{13}C]glucose tracer in a KP-derived cell line, related to Figure 4.

Fragment	Mass Isotopomer	Measured	Simulated
Lac261	M+0	0.393867	0.391014
	M+1	0.115467	0.118052
	M+2	0.3677	0.368017
	M+3	0.084333	0.084138
	M+4	0.032833	0.032748
	M+5	0.0048	0.005045
	M+6	0.0009	0.000887
	M+7	0	9.1E-05

SUPPLEMENTAL EXPERIMENTAL PROCEDURES

Mouse Lung Cancer Models

All animal studies were approved by the MIT Committee on Animal Care. For all studies, animals were placed randomly into groups before collecting data or administering treatments. Mice were housed under standard 12-hr light/dark cycles and fed RMH 3000 (Prolab) *ad-libitum* until 6-hours before infusions. For the LA2 model (Johnson et al., 2001) we used four to six-month old mice from a mixed 129/Sv and B6 genetic background. For KP mouse studies, we initiated tumors in two to six-month old mice from a mixed 129/Sv and B6 genetic background by intratracheal administration of 2.5x107 PFU of adenovirus with Cre-recombinase (Gene Transfer Vector Core, University of Iowa). For allograft and xenograft studies, two to four month old C57Bl6/J or nu/nu mice were used.

Orthotopic/Allograft Induction in Mice

For orthotopic transplant tumors, cells were grown to 70% confluence and resuspended in PBS. Cells were injected at a concentration of $7x10^4$ cells/50μL intratracheally through a 25-gauge catheter to seed cell in the lung directly in 12 week C57Bl6 (Line 1) or nu/nu (Line 2) mice. For allograft tumors, cells were grown to 70% confluence and resuspended in PBS. These were injected at $2x10^5$/100μL in flanks of C57Bl6 (Line 1) or nu/nu (Line 2) mice. Tumor growth in allograft flanks were measured with calipers and volumes estimated with the formula $(\pi/6)(L \times W^2)$. Graphs with identical control curves represent experiments performed in parallel in the same cohort of mice.

Glucose and Glutamine Infusions in Mice

Arterial and venous catheters were surgically implanted into the jugular veins and/or carotid artery of normal or tumor bearing animals 3-4 days prior to infusions. Animals were fasted for 6-hrs (morning fast) and infusions were performed in free-moving, conscious animals at 1:00pm for all studies to minimize metabolic changes associated with circadian rhythm. A constant infusion of [U-^{13}C]glucose

(30mg/kg/min, unless otherwise specified to be 20mg/kg/min) or [U-^{13}C]glutamine (LA2 tumor-bearing mice infused at 2.0mg/kg/min, KP, KPS, and xenografted A549 and H1975 tumor-bearing mice infused at 3.7mg/kg/min) (Cambridge Isotopes Laboratories) was administered for a 6-hour duration. Animals were terminally anesthetized with 120mg/kg sodium pentobarbital and all tissues were harvested in less than 5 minutes. Following microdissection, tumors and adjacent lung tissue was rapidly frozen using a BioSqueezer (BioSpec Products) to ensure rapid quenching of metabolism. Tissues were stored at -80°C and subsequently processed for metabolite extraction and analysis.

Cell Culture

Cell lines from tumors arising from the KP lung cancer model were established by digestion of tumors in collagenase IV/dispase for 30 min at 37°C in 1mL of trypsin and propagated in DMEM without pyruvate containing 10% FBS, 2mM glutamine, 100U/mL penicillin, 100μg/uL streptomycin at 21% oxygen. Isogenic clones were selected for comparison of CRISPR cell lines. For labeling studies and MFA, cells were seeded at an initial density of 150,000 cells/well in DMEM and changed to glucose or glutamine-free DMEM and grown for 24 hours in media containing 17.5mmol/L [U-^{13}C]glucose, [1,2-^{13}C]glucose, or 4mmol/L [U-^{13}C]glutamine (Cambridge Isotopes Laboratories). For labeling in 3D culture, cells were seeded at an initial density of 150,000 cells/well of Low Adherence plates (Corning) in DMEM + 2% matrigel and changed to glucose or glutamine-free DMEM and grown for 24 hours in media containing 17.5mmol/L [U-^{13}C]glucose, [1,2-^{13}C]glucose, or 4mmol/L [U-^{13}C]glutamine (Cambridge Isotopes Laboratories). Cells in 3D were quantified using CellTiter-Glo (Promega) after establishing intracellular ATP concentration is linear with cell number.

Metabolite Extractions

Tissues were weighed (wet tissue weight) and homogenized cryogenically (Retsch Cryomill). Metabolites were extracted from tissues weighing between 10-40mg in a chloroforom:methanol:water extraction solution at a volume ratio of 400:600:300. Samples were vortexed and centrifuged at 10,000xg for 10min to separate aqueous and organic layers. Polar metabolites were dried under nitrogen gas and frozen at -80C for subsequent analysis by liquid or gas-chromatography mass-spectrometry.

LC-MS Measurements from [U-^{13}C]glucose, [U-^{13}C]glutamine, and CB-839 labeling experiments

Frozen and dried metabolites were resuspended in water based on tissue weight with valine-D8 included as an injection control. Liquid chromatography tandem mass spectrometry (LC-MS) metabolomics profiling plasma and tissue profiles were measured using a combination of two LC-MS methods designed to measure polar metabolites. Negative and positive ionization mode analyses of

polar metabolites were acquired using an LC-MS system comprised of a Nexera X2 U-HPLC (Shimadzu, Marlborough, MA) and a Q-Exactive hybrid quadrupole orbitrap mass spectrometer (Thermo Fisher Scientific; Waltham, MA). Samples for positive ion mode, polar metabolite analyses were prepared and separated using the same hydrophobic interaction liquid chromatography method (HILIC) as described previously (Townsend et al., 2013; Wang et al., 2011) and MS data were acquired over m/z 70-800. Samples for negative ion mode analyses of polar metabolites were achieved using a HILIC method under basic conditions as described previously (Avanesov et al., 2014) and MS data were acquired over m/z 70-750. MS data were processed using Tracefinder (version 3.2, Thermo Fisher Scientific; Waltham, MA). Two LC-MS methods were used to measure polar metabolites in plasma and tissues. All data were acquired using an LC-MS system comprised of a Nexera X2 U-HPLC (Shimadzu, Marlborough, MA) and a Q Exactive hybrid quadrupole orbitrap mass spectrometer (Thermo Fisher Scientific; Waltham, MA). Hydrophilic interaction liquid chromatography (HILIC) analyses of water soluble metabolites in the positive ionization mode were carried out by extracting 10 µl homogenate using 90 µl of 74.9:24.9:0.2 vol/vol/vol acetonitrile/methanol/formic acid containing stable isotope-labeled internal standards (valine-d8, Isotec; and phenylalanine-d8, Cambridge Isotope Laboratories; Andover, MA). The samples were centrifuged (10 min, 9000×*g*, 4°C) and the supernatants were injected directly onto a 150 × 2 mm Atlantis HILIC column (Waters; Milford, MA). The column was eluted isocratically at a flow rate of 250 µl/min with 5% mobile phase A (10 mM ammonium formate and 0.1% formic acid in water) for 1 min followed by a linear gradient to 40% mobile phase B (acetonitrile with 0.1% formic acid) over 10 min. The electrospray ionization voltage was 3.5 kV and data were acquired using full scan analysis over m/z 70–800 at 70,000 resolution and a 3 Hz data acquisition rate. Negative ion mode analyses of polar metabolites were achieved using a HILIC method under basic conditions. Briefly, 30 µl homogenate was extracted using 120 µl of 80% methanol containing [^{15}N]inosine, thymine-d4, and glycocholate-d4 internal standards (Cambridge Isotope Laboratories; Andover, MA). The samples were centrifuged (10 min, 9000×*g*, 4°C) and the supernatants were injected directly onto a 150 × 2.0 mm Luna NH2 column (Phenomenex; Torrance, CA) that was eluted at a flow rate of 400 µl/min with initial conditions of 10% mobile phase A (20 mM ammonium acetate and 20 mM ammonium hydroxide in water) and 90% mobile phase B (10 mM ammonium hydroxide in 75:25 vol/vol acetonitrile/methanol) followed by a 10 min linear gradient to 100% mobile phase A. MS full scan data were acquired over m/z 70–750. The ionization source voltage is −3.0 kV and the source temperature is 325°C.

GC-MS Measurements of [U-^{13}C]glucose and [U-^{13}C]C-glutamine labeled metabolites

Frozen and dried tissue metabolites were dissolved in 10μL/10mg of wet weight of tissue extracted of 2% methoxyamine hydrochloride in pyridine (Sigma) and held at 37C for 1.5h. Tert-butyldimethylsilyl derivatization was initiated by adding 15μL/10mg of wet weight of extracted tissue of N-methyl-N-(tert-butyldimethylsilyl)trifluoroacetamide + 1% tert-butyldimethylchlorosilane (Sigma) and incubated at 37C for 1hr. GC-MS analysis was performed using an Agilent 7890 GC equipped with 30m DB-35MS capillary column connected to an Agilent 5975B MS operating under electron impact ionization at 70eV. One microliter of sample was injected in splitless mode at 270C, using helium as a carrier gas at a flow rate of 1mL min^{-1}. For measurement of polar metabolites, the GC oven temperature was held at 100C for 3mins and increased to 300C at 3.5C min^{-1}. The MS source and quadrupole were held at 230C and 150C, respectively, and the detector was run in scanning mode, recording ion abundance in the range of 100-605m/z. MIDs were determined by integrating the appropriate ion fragments and correct for natural isotope abundance using in house algorithms adapted as previously reported using norvaline as an internal injection control (Commisso et al., 2013).

Extracellular Flux Measurements

Extracellular flux measurements were calculated by extracting fresh and spent medium supernatant from tracing experiments after 24 hours of growth. Cells were assumed to grow exponentially over the culture period. Glucose, lactate, glutamine, and glutamate were measured using YSI biochemistry analyzer (Yellow Springs Instruments, Yellow Springs, OH).

Enzyme-linked Immunosorbent Assay (ELISA) and Glucometer Measurements

Plasma was collected from an arterial catheter during venous glucose infusions in EDTA-coated tubes, aliquoted, and frozen at −80°C for further analysis. Plasma insulin levels were determined using an ultrasensitive mouse insulin ELISA kit (Crystal Chem, #90080). Blood glucose levels from the same mice were measured using a handheld glucometer (One Touch).

Micro Computed Tomography Imaging

Animals were anesthetized with 2% isofluorane, oxygen mixture and underwent μCT scanning in a eXplore CT120-whole mouse μCT (GE Healthcare). Volume measurements were quantified using MicroView 3D Image Viewing (Parallax-Innovations) and representative coronal Z-stacks were extracted using OsiriX (OsiriX-Viewer).

Metabolic Flux Analysis

^{13}C-assisted metabolic flux analysis (MFA) was used to estimate the fates of intracellular pyruvate in KP-derived mouse lung cancer cell lines. An in-house, elementary-metabolite-unit-based software (Antoniewicz et al., 2006, 2007) was used to generate a set of flux values and 95% confidence intervals corresponding to a simplified model of central carbon metabolism (Table S3). The software, which was run in Matlab v2009b (Mathworks), minimizes the lack of fit between measured data (extracellular fluxes and intracellular metabolite labeling patterns) and simulated data corresponding to potential flux distributions, as described elsewhere (Antoniewicz et al., 2006; Wiechert et al., 2001). Flux estimation was performed 500 times, each with randomly chosen initial values, and the flux distribution with the lowest weighted sum of squared errors was that corresponding to the global minimum.

Measured glucose consumption, lactate production, glutamine consumption, and proliferation were used to constrain the flux distribution (Table S5). The intracellular metabolite fragment labeling patterns (Table S6) used in the analysis were Pyr174, Lac233, Lac261, Ala260, Mal419, Asp302, Asp390, Asp418, Glu330, Glu432, Cit459, and Cit591, as these were found to give sufficient resolution for estimating pyruvate-consuming fluxes with a [U-^{13}C]glutamine tracer (Table S4). In addition, the Lac261 labeling pattern from a [1,2-^{13}C]glucose tracer was used to resolve pentose phosphate pathway fluxes (Table S7) (Metallo et al., 2012). The following assumptions were made for the analysis:

1. Cells were cultured in media containing the ^{13}C tracer for 24 h before harvesting, at which point the system was assumed to be at pseudo-steady state for both metabolic fluxes and isotopic-labeling patterns of metabolites were attained, enabling the use of steady state MFA (Wiechert and de Graaf, 1996). Changes in TCA cycle metabolite or lactate labeling patterns following 24-h culture in [U-^{13}C]glutamine or [1,2-^{13}C]glucose, respectively, have previously been shown to be negligible (Ahn and Antoniewicz, 2011, 2013; Metallo et al., 2012). Cells were in the exponential growth phase during the labeling period.
2. Dissolved CO_2 freely exchanges with gaseous CO_2. Unlabeled CO_2 can be used in carboxylation reactions, but evolved CO_2 resulting from loss of ^{13}C atoms can also be reincorporated for carboxylation reactions, if necessary.
3. Pyruvate, malate, citrate, α-ketoglutarate, and aspartate exist in separate mitochondrial and cytosolic pools, where they participate in distinct chemical reactions and become differentially labeled, but can be transported freely between intracellular compartmental. The measured metabolite labeling patterns results from the mixture of these two pools. Other metabolites may exist in both pools, but rapid equilibration between the pools in a manner that precludes distinct labeling patterns was assumed.

4. Succinate and fumarate are symmetric metabolites, so their interconversion scrambles the first- and second-carbon labeling states with the third- and fourth-carbon labeling states, respectively.
5. Because anabolic fluxes that contribute to biomass fluxes are small relative to others in central carbon metabolism, the expected flux distribution is largely insensitive to the assumed biomass composition (Folger et al., 2011; Frezza et al., 2011). Correspondingly, the biomass equation used here is only approximate. Dry cell weight is predominantly protein, so the core biomass equation was assumed to consist of nonessential amino acids primarily synthesized by intracellular central carbon metabolites in DMEM culture conditions; this led to the inclusion of aspartate, glutamate, glutamine, and alanine. Asparagine (which is synthesized from aspartate) and proline (which is synthesized from glutamate) were included with aspartate and glutamate respectively. Serine, glycine, and cysteine were not included as they were assumed to be derived primarily from the media. Dihydroxyacetone phosphate (DHAP) and cytosolic acetyl CoA were also considered to account for lipid synthesis, and pentose 5-phosphate (P5P) was considered to account for nucleotide synthesis. Literature reports of biomass composition for hybridoma cells was used as an estimate for the relative sizes of these demands (Sheikh et al., 2005), and these were scaled to give units of fmol/cell by assuming each cell weighs 150 pg (Murphy et al., 2013).
6. The uncertainties of extracellular fluxes were set to their measured standard deviations. The uncertainties of metabolite isotopomer mole fractions were set to 0.35 mol %, which is consistent with typical measurement and modeling errors (Wasylenko et al., 2015; Wasylenko and Stephanopoulos, 2015).

sgRNAs and Primers Used for the Generation of Knockout Cell Lines and Tumors

sgRNAs were designed using E-CRISP (e-crisp.org) to *Pdha1*, *Pcx*, and *Gls1* with restriction enzyme compatible sites and a G was added to the +1 position where not already present for U6 transcription. sgRNAs were introduced into the U6-sgRNA-EFS-Cas9-2A-Puro vector for generation of cell lines or U6-sgRNA-EFS-Cas9-2A-Cre (pSECC) for use *in vivo* using BsmBI as previously described (Sánchez-Rivera et al., 2014). Lentivirus was produced by co-transfection of 293T cells with packaging constructs (delta8.2 and VSV-G) using TransIT-LT1 (Mirus Bio). Supernatant was concentrated by ultracentrifugation, resuspended in OptiMEM (Gibco), and animals were infected with pSECC to disrupt *Gls1, Pcx,* or *Pdha1* concomitantly with Cre activation to initiate tumors as described previously (Sánchez-Rivera et al., 2014).

Guide sequences, guide sequence exon target, and verification primers used to make knockout cell lines for *Pcx*, *Pdha1*, and *Gls1*, and used with pSECC to knockout genes in tumors and Protospacer adjacent motif (PAM) with sequence NGG in bold.

sgRNA Sequences

Target Gene	sgRNA ID	Sequence of sgRNA	Strand	Exon
Pdha1	sgPdha1	GCGCAGAGCCTGCCAACACG**CGG**	-	1
Pcx	sgPcx.1	GCCTATCAAGAAAGTAATGG**TGG**	+	1
Pcx	sgPcx.2	CTCCCCAAATGTCCGGCGTC**TGG**	+	1
Gls1	sgGls1.1	CCGCGCCGGGGCCCTTCGCG**CGG**	+	1
Gls1	sgGls1.2	CCTTGCTGAAAAGAAATGAA**AGG**	+	1

Verification Primers

Primer ID	Primer Sequence	Exon Amplified
Pdha1-F	TAAGGGACGAGCAGTTGTG	1
Pdha1-R	CTCCTTTTGAGTGCCTGGGT	1
Pcx-F	AGACTCTGATTGCCCCTCCT	1
Pcx-R	TGTCCTGCTCCGAGTAGACA	1
Gls1-F	TTTCTCTTCCGCGAACCTCC	1
Gls1-R	TTGAGCGTCAGTCTCAGTGC	1

SUPPLEMENTAL REFERENCES

Ahn, W.S., and Antoniewicz, M.R. (2011). Metabolic flux analysis of CHO cells at growth and non-growth phases using isotopic tracers and mass spectrometry. In Metabolic Engineering, pp. 598-609.
Ahn, W.S., and Antoniewicz, M.R. (2013). Parallel labeling experiments with [1,2-(13)C]glucose and [U-(13)C]glutamine provide new insights into CHO cell metabolism. In Metabolic Engineering, pp. 34-47.

Antoniewicz, M.R., Kelleher, J.K., and Stephanopoulos, G. (2006). Determination of confidence intervals of metabolic fluxes estimated from stable isotope measurements. In Metabolic Engineering, pp. 324-337.

Antoniewicz, M.R., Kelleher, J.K., and Stephanopoulos, G. (2007). Elementary metabolite units (EMU): a novel framework for modeling isotopic distributions. In Metabolic Engineering, pp. 68-86.
Avanesov, A.S., Ma, S., Pierce, K.A., Yim, S.H., Lee, B.C., Clish, C.B., and Gladyshev, V.N. (2014). Age- and diet-associated metabolome remodeling characterizes the aging process driven by damage accumulation. In Elife, pp. e02077-e02077.

Commisso, C., Davidson, S.M., Soydaner-Azeloglu, R.G., Parker, S.J., Kamphorst, J.J., Hackett, S., Grabocka, E., Nofal, M., Drebin, J.A., Thompson, C.B.*, et al.* (2013). Macropinocytosis of protein is an amino acid supply route in Ras-transformed cells. In Nature, pp. 633-637.

Folger, O., Jerby, L., Frezza, C., Gottlieb, E., Ruppin, E., and Shlomi, T. (2011). Predicting selective drug targets in cancer through metabolic networks. In Mol Syst Biol, pp. 501-501.

Frezza, C., Zheng, L., Folger, O., Rajagopalan, K.N., MacKenzie, E.D., Jerby, L., Micaroni, M., Chaneton, B., Adam, J., Hedley, A.*, et al.* (2011). Haem oxygenase is synthetically lethal with the tumour suppressor fumarate hydratase. In Nature, pp. 225-228.

Metallo, C.M., Gameiro, P.A., Bell, E.L., Mattaini, K.R., Yang, J., Hiller, K., Jewell, C.M., Johnson, Z.R., Irvine, D.J., Guarente, L.*, et al.* (2012). Reductive glutamine metabolism by IDH1 mediates lipogenesis under hypoxia. In Nature, pp. 380-384.

Murphy, T.A., Dang, C.V., and Young, J.D. (2013). Isotopically nonstationary 13C flux analysis of Myc-induced metabolic reprogramming in B-cells. In Metabolic Engineering, pp. 206-217.

Sánchez-Rivera, F.J., Papagiannakopoulos, T., Romero, R., Tammela, T., Bauer, M.R., Bhutkar, A., Joshi, N.S., Subbaraj, L., Bronson, R.T., Xue, W.*, et al.* (2014). Rapid modelling of cooperating genetic events in cancer through somatic genome editing. In Nature, pp. 428-431.

Sheikh, K., Förster, J., and Nielsen, L.K. (2005). Modeling hybridoma cell metabolism using a generic genome-scale metabolic model of Mus musculus. In Biotechnol Prog, pp. 112-121.

Townsend, M.K., Clish, C.B., Kraft, P., Wu, C., Souza, A.L., Deik, A.A., Tworoger, S.S., and Wolpin, B.M. (2013). Reproducibility of metabolomic profiles among men and women in 2 large cohort studies. In Clin Chem, pp. 1657-1667.

Wang, T.J., Larson, M.G., Vasan, R.S., Cheng, S., Rhee, E.P., McCabe, E., Lewis, G.D., Fox, C.S., Jacques, P.F., Fernandez, C.*, et al.* (2011). Metabolite profiles and the risk of developing diabetes. In Nat Med, pp. 448-453.

Wasylenko, T.M., Ahn, W.S., and Stephanopoulos, G. (2015). The oxidative pentose phosphate pathway is the primary source of NADPH for lipid overproduction from glucose in Yarrowia lipolytica. In Metabolic Engineering, pp. 27-39.

Wasylenko, T.M., and Stephanopoulos, G. (2015). Metabolomic and (13)C-metabolic flux analysis of a xylose-consuming Saccharomyces cerevisiae strain expressing xylose isomerase. In Biotechnol Bioeng, pp. 470-483.

Wiechert, W., and de Graaf, A.A. (1996). In vivo stationary flux analysis by 13C labeling experiments. In Adv Biochem Eng Biotechnol, pp. 109-154.

Wiechert, W., Möllney, M., Petersen, S., and de Graaf, A.A. (2001). A Universal Framework for 13C Metabolic Flux Analysis. In Metabolic Engineering, pp. 265-283.